Universidad de Cantabria

Facultad de Ciencias

ON LIGHT SCATTERING BY NANOPARTICLES WITH CONVENTIONAL AND NON-CONVENTIONAL OPTICAL PROPERTIES

PH.D. THESIS

Braulio García-Cámara

Santander, July 2010

Part I

Study of the Scattering Properties of an Isolated Particle

3

Light Scattering Resonances by Small Particles with Electric and Magnetic Properties

"No te puedes poner ningún límite, no hay nada imposible"
—Usain Bolt, 1986- , velocista jamaicano

3.1. Introduction

Advances in nanophotonics offer new technical possibilities like intra-chip optical communications [7, 32, 98] or biosensors [10, 144, 81, 78]. Thereto smaller component sizes and nobel behaviors are required, such as high optical response or directional control of the light scattering (waveguiding). This brought researchers to concentrate on systems much smaller in size than those considered a few years ago. Technological advances have allowed to obtain well-defined structures and particles in the nanometric range [133, 75, 141]. For such systems, the scattering cross-section is usually very small, which is a huge inconvenient for structures which are supposed to affect or alter the propagation of light. This problem can be overcome if scatterers can sustain resonances which enhance light-matter interaction. In this context, metallic nanostructures have received a lot of attention due to their ability to

confine electromagnetic waves to regions in space much smaller than the wavelength (below the classical diffraction limit) by means of **localized surface plasmons** [118]. As was commented before, these surface plasmons are collective oscillation of the electron plasma at the interface between a metal and a dielectric, or in other words, on the surface of the metallic nanostructures.

Light scattering resonances can also appear in non-metallic structures and have been studied for a long time. As an example we would like to mention the work done by G. Videen and W. Bickel [139]. They analyzed Mie resonances for very small dielectric ($\epsilon > 0$, $\mu = 1$) spherical particles and made a complete study of resonances as a function of particle size and the refractive index of the scatterer. As the considered particles are much smaller than the incident wavelength, some approximations to Mie theory can be used. The authors showed that Mie coefficients of order higher than 2 can be neglected. Furthermore, they proposed approximate expressions for the first four Mie coefficients a_1, a_2, b_1 and b_2 (see equations (2.63), (2.64) and (2.65)).

In addition to this, the new engineered materials or metamaterials [129] which present effective optical properties have extended the range of values that the electric permittivity (ϵ) and the magnetic permeability (μ) can reach. Special attention has been dedicated to the case of negative electric permittivity ($\epsilon < 0$) and negative magnetic permeability ($\mu < 0$). This is the so-called double-negative or left-handed range ($\epsilon < 0$ and $\mu < 0$), for which light propagation present some interesting characteristics [128].

Those new materials have created the possibility to obtain, in theory, arbitrary values of the refractive index and hence, different and new scattering behaviors such as resonant features. In this section and in collaboration with Prof. Videen, we have generalized the previous analysis [139] about the resonances in dielectric particle but now without any restriction on the values of the optical properties. Furthermore, the evolution of these resonances, in particular their position and width, as a function of the optical properties and of particle size have been described.

3.2. Mie Resonances

As it is well-known, light scattering by a particle depends on the size, shape and optical properties of the scatterer as well as the frequency of the incident wave. In the same way, resonances and their spectral properties (peak width and position) depend also on particle size and optical properties. From a mathematical point of view, resonances are excited when

the denominator of the Mie coefficients, (2.31) and (2.32), are zero. For particles in the Rayleigh limit ($x \to 0$) the zeros of the denominator of a_n and b_n appear when [14]

$$m^2 = -\frac{n+1}{n}, \quad n = 1, 2... \tag{3.1}$$

Being m the refractive index of the particle relative to the surrounding medium. For a non-magnetic particle ($\mu = 1$) with an electric permittivity $\epsilon = \epsilon' + i\epsilon''$ immersed in a non-absorbing surrounding medium (ϵ_m) and for the first order case ($n = 1$) the resonant behavior appears for

$$\epsilon' = -2\epsilon_m \text{ and } \epsilon'' = 0 \tag{3.2}$$

This resonance is known as *Fröhlich resonance* or *mode of uniform polarization*[14].

In the previous section, new and generalized expressions for a_1, a_2, b_1 and b_2 were presented (equations (2.66) and (2.67)), following the approximations derived by G.Videen and W. Bickel but including the possibility of $\mu \neq 1$. Using these expressions, in this section we generalize the analysis of the Mie resonances for small but finite size particles as a function of the optical properties and their size. For this study we have calculated the spectral characteristics of the extinction efficiency to analyze the position and width of the resonant modes. As we have considered particle sizes in the range ($R \in [0.01\lambda - 0.1\lambda]$), Mie coefficients of order higher than two can be neglected and only the first four terms are retained. Under these considerations the extinction efficiency can be written as

$$Q_{ext} = \frac{2}{x^2}[3Re(a_1 + b_1) + 5Re(a_2 + b_2)] \tag{3.3}$$

In what follows, we will refer to a_1 and a_2 as the electric terms (dipolar and quadrupolar respectively) and to b_1 and b_2 as magnetic terms (dipolar and quadrupolar respectively). Resonant modes appearing due to zeros in the denominator of one these coefficients will be called in the same way. For instance, a mode due to a zero in the denominator of a_1 will be called dipolar electric resonance.

3.3. Dependence of Mie Resonances with the Optical Properties

The purpose of this section is to analyze the dependence of the resonances of a small particle with its optical properties. The difference of this work with respect to previous ones [139], lays in the fact that now arbitrary values for the electric permittivity and the magnetic permeability, either positive and negative are considered.

In Figure 3.1, we plot Q_{ext} (semi-logarithmic scale) for spherical particles as a function of the optical properties (ϵ and μ). The particle size ($R = 0.01\lambda$) was chosen very small compared with the incident wavelength, in such a way that the expressions (2.66), (2.67) and the corresponding ones for b_1 and b_2 reproduce accurately the cross-sections. The values for the electric permittivity were chosen in order to be comparable with those in [139]. While the range of values for the magnetic permeability was chosen not to be huge but enough to observe the main resonances.

For a detailed analysis, we have considered separately four different cases that coincide with the four quadrants in $\epsilon - \mu$ representation: i) ($\epsilon > 0$ and $\mu > 0$), ii) ($\epsilon < 0$ and $\mu > 0$), iii) $\epsilon < 0$ and $\mu < 0$, and iv) $\epsilon > 0$ and $\mu < 0$. In the first case, the conventional dielectric materials for the visible with $\epsilon > 0$ and $\mu = 1$ are included. The second case includes metallic materials ($\epsilon < 0$ and $\mu = 1$) while the third one represents left-handed materials ($\epsilon < 0$, $\mu < 0$ and then $m < 0$). Finally, the last case does not have any physical interest at present, but it cannot be excluded from a complete study.

Case $\epsilon > 0$ and $\mu > 0$ (Figure 3.1b): First, we reproduced for $\epsilon > 0$ and $\mu = 1$, the typical Mie resonances as represented in Figure 1 of [139]. We analyzed the evolution of the position of these resonances as the magnetic permeability (μ) changes. In Figure 3.2(a) it can be seen that the resonances are organized in branches, having an origin in the electric or magnetic terms depending on the values of ϵ and μ. Each resonance, and then each branch, matches with maximum values of a scattering coefficient. In Figure 3.2(a), the corresponding coefficient is shown.

As can be observed, the evolution of the resonance's position is such that as μ increases, the resonance appears for smaller values of $|\epsilon|$. There is no difference between the resonances and every one of them show the same evolution.

Case $\epsilon < 0$ **and** $\mu > 0$ (Figure 3.1a): In this domain, only the Mie coefficients a_1 and a_2 may take high values, which implies that only electric resonances (dipolar and quadrupolar) can be excited. The dipolar resonance, associated to maximum values of a_1, appears around $\epsilon \simeq -2$. Only when the particle size tends to zero (dipole-like particle), the resonant position is exactly $\epsilon = -2$. This resonance is the Frölich resonance described in (3.2) which is slightly shifted due to the quadrupolar effects (a_2). Although the particle size is small, quadrupolar effects can be observed. In this domain an electric quadrupolar resonance can be observed at $\epsilon \simeq -1.5$, and it is associated to high values of the coefficient a_2.

Resonances in this domain do not change (or only a little) their spectral position as the magnetic permeability changes.

Case $\epsilon < 0$ **and** $\mu < 0$ (Figure 3.1c): This could be the most interesting region due to the amount of features that can be observed here. Additionally, this range corresponds to a negative refractive index [138]. While these values of the electric permittivity and the magnetic permeability cannot be found in naturally occurring materials, recent developments have permitted to build structures presenting effective optical constants in this range [128, 135, 15].

We can distinguish two different behaviors in this quadrant: for low values of the modulus of the electric permittivity ($|\epsilon| \leq 10$) and for larger values ($|\epsilon| \geq 10$). The first case is enlarged in Figure 3.2(b). Here, both electric and magnetic resonances can be observed. The electric ones are a continuation of those described in the previous case. The dipolar electric resonance appears at $\epsilon \simeq -2$ for every value of the magnetic permeability, while the quadrupolar electric mode is located at $\epsilon \simeq -1.5$, and remains fixed as μ changes. Two additional resonances can be observed. These are associated with the magnetic coefficients, b_1 and b_2. The dipolar magnetic mode that correspond to high values of b_1, at $\mu \simeq -2$ and the quadrupolar one (associated to b_2), at $\mu \simeq -1.5$. Only when $R \to 0$, resonances appear at the exact values. As happens for the electric resonances, these modes remain fixed for every value of the electric permittivity in the considered range. An interesting $\epsilon - \mu$ symmetry is observed in this domain: the values of ϵ at which the electric resonances appear, are equal to those values of μ at which the magnetic modes are observed. This symmetry is connected to that observed for the Mie coefficients under the Rayleigh approximation (See equations (2.56) and (2.57)). Here, we see that this symmetry is still present when the Rayleigh approximation is not strictly valid anymore and that it can be extended to

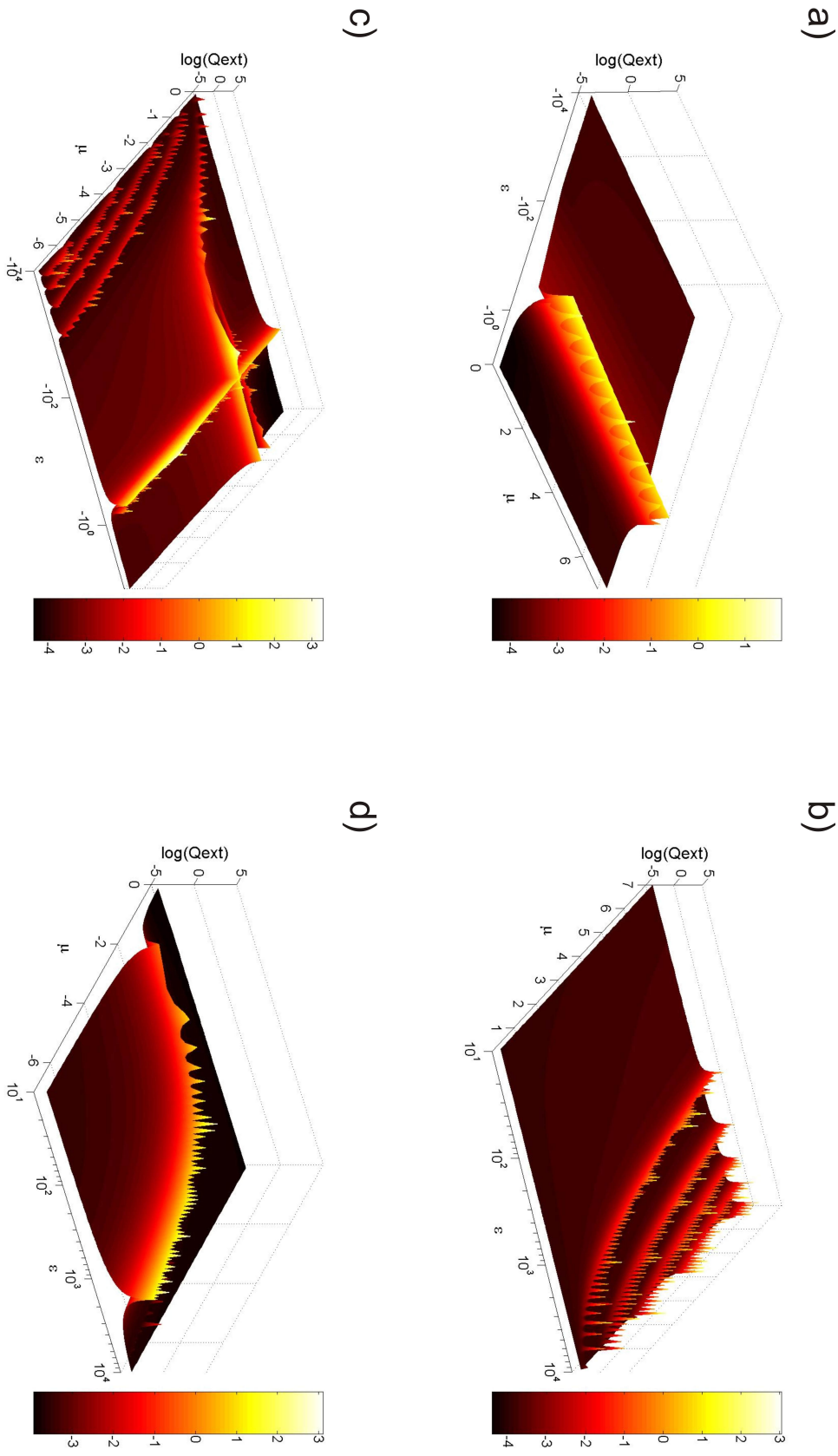

Figure 3.1: 3D plots of $\log(Q_{ext})$ as a function of the optical properties (ϵ and μ)for a spherical particles of $R = 0.01\lambda$

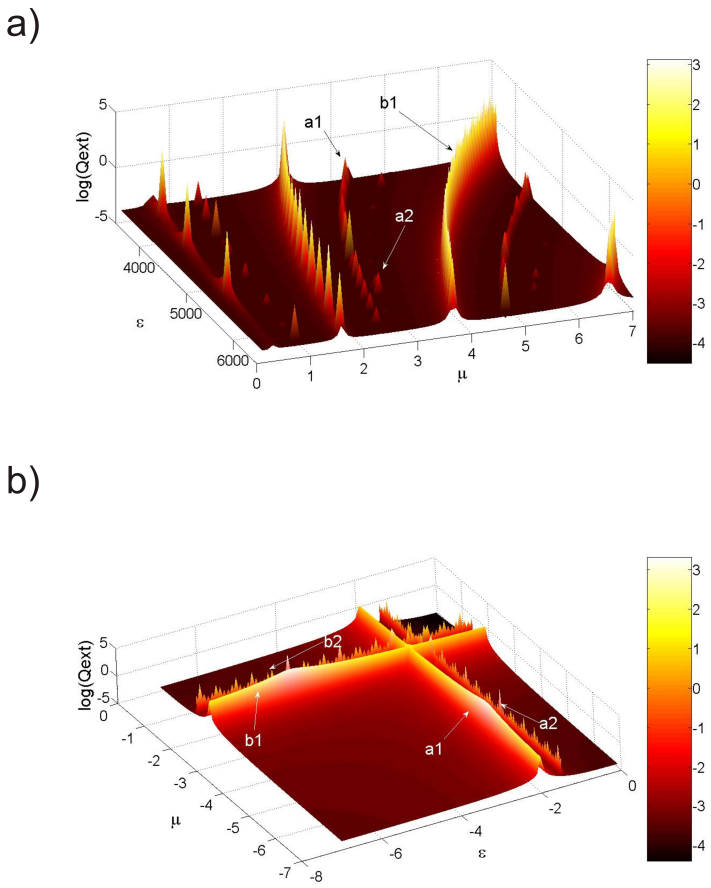

Figure 3.2: Enlargement of two interesting zones of Figure3.1: (a) Region with $\epsilon > 0, \mu > 0$; (b)Region with $\epsilon < 0, \mu < 0$. The coefficient that takes the highest values when the resonance is excited is indicated.

the quadrupolar terms. The dipolar resonances, both electric and magnetic, present a particular structure with a high intense background and a peak that appears at $\mu = -5$ for the electric case and at $\epsilon = -5$ for the magnetic one, as depicted in Figure 3.2(b).

For larger values of the electric permittivity ($|\epsilon| > 10^2$) similar resonances to those observed for $\epsilon > 0, \mu > 0$ are found. Also, their behavior as the magnetic permeability changes is also very similar to that of the modes in the first case ($\epsilon > 0$, $\mu > 0$): increasing the modulus of the magnetic permeability shifts the position of each resonance to lower values of the modulus of the electric permittivity ($|\epsilon|$).

Case $\epsilon > 0$ **and** $\mu < 0$ (Figure 3.1d): This range is the most unusual as compared with the previous cases. The interval we are considering here is not related with any natural or engineered material. Nevertheless, the rapid advances obtained in the field of metama-

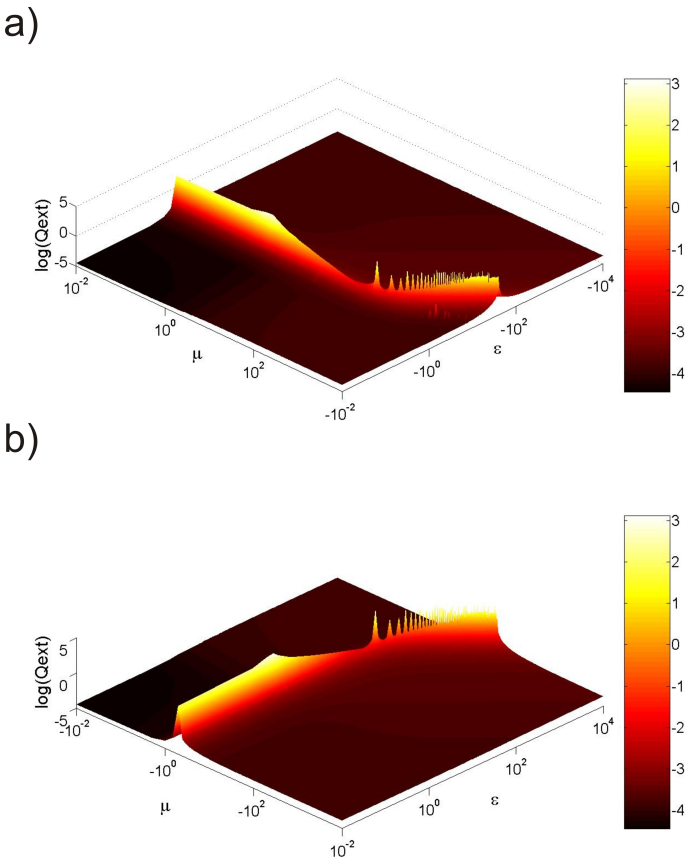

Figure 3.3: 3D plots of Q_{ext} for a spherical particle ($R = 0.01\lambda$) as a function of the optical properties (ϵ and μ) for two different ranges:(a) $\epsilon < 0$, and $\mu > 0$; (b) $\epsilon > 0$, and $\mu < 0$ when the range of values for ϵ and μ is the same.

terials, could produce them in a near future. For this reason and in order to complete this study, we include this possibility.

Here, only magnetic modes are excited: the magnetic dipolar resonance, associated to b_1, and the magnetic quadrupolar resonance, related to b_2. These resonances appear as a continuation of the magnetic modes appearing in the previous case. They are located at $\mu \simeq -2$ for the dipolar resonances and at $\mu \simeq -1.5$ for the quadrupolar one. However, for high values of the electric permittivity, the behavior of the resonances' positions is more complex.

Again, a $\epsilon - \mu$ symmetry is observed for the electric and magnetic resonances in the range ($\epsilon < 0, \mu < 0$) according to the symmetry of the Mie coefficients (equations (2.56) and (2.57)). We have already commented that the electric resonances in the second case ($\epsilon < 0, \mu > 0$) and the magnetic ones in this section ($\epsilon > 0, \mu < 0$), seem to be a continuation of those symmetric resonances in ($\epsilon < 0, \mu < 0$). A question that has to be raised is whether the electric and magnetic resonances of these ranges present a similar $\epsilon - \mu$ symmetry. To analyze this, we plot in Figure 3.3, the extinction efficiency (Q_{ext}) of a spherical particle ($R = 0.01\lambda$) as a function of the optical properties in these two regions ($\epsilon < 0, \mu > 0$ and $\epsilon > 0, \mu < 0$) when the range for ϵ and μ is the same. It can be seen that the behavior is symmetric: the electric resonances in Figure 3.3(a) depend on ϵ in the same way as the magnetic resonances depends on μ in Figure 3.3(b).

3.4. Dependence of Mie Resonances with the Particle Size

In the previous section, we have considered particle sizes that are much smaller than the wavelength of the incident radiation. It is evident that the spectral behavior of the cross-sections (extinction, absorption and scattering) will depend, among other parameters, on the particle size. The purpose of this section is to analyze this size-dependence. In Figure 3.4 the logarithm of Q_{ext} is plotted for several particle sizes and for two different cases:

(a) as a function of the electric permittivity and $\mu = -2$. In this case, the electric resonances are excited. The peak associated to the dipolar magnetic term (b_1) is also shown.

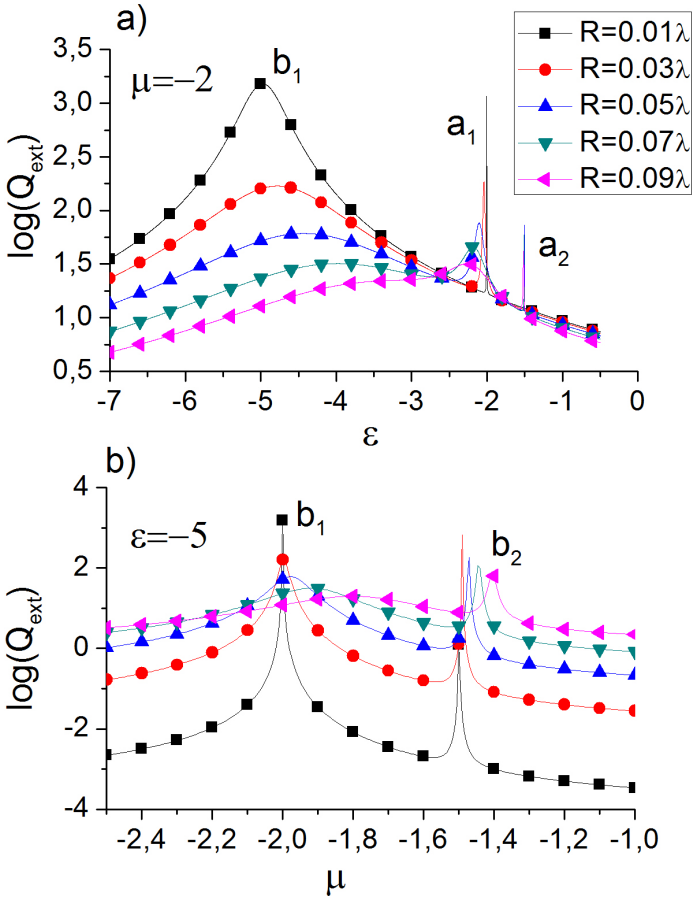

Figure 3.4: Evolution of the extinction efficiency, in semilogarithmic scale, as a function of (a) the electric permittivity and (b) the magnetic permeability in the negative-negative range for several values of the particle size. The value of (a) μ and (b) ϵ is indicated in the upper left corner. Some resonances are excited in this range which are labeled with the corresponding Lorenz-Mie coefficient

(b) as a function of the magnetic permeability and $\epsilon = -5$ (remember the structure of the electric resonances). In this case, normal sections of the magnetic resonances can be observed.

In Figure 3.4(a) and for very small particles ($R = 0.01\lambda$), only dipolar resonances appear: the electric one is located at $\epsilon \cong -2$, where high values of a_1 are reached, another peak due to a magnetic contribution is also observed at $\epsilon \cong -5$. As R increases, these two peaks evolve becoming broader and shifted, Q_{ext} takes lower values and new resonances of higher orders appear. In particular, an electric quadrupolar resonance, related to high values of a_2, comes into sight at $\epsilon \cong -1.5$. For higher values of the particle size, the dipolar resonances tend to disappear, becoming less sharp until only the quadrupolar resonance remains as a

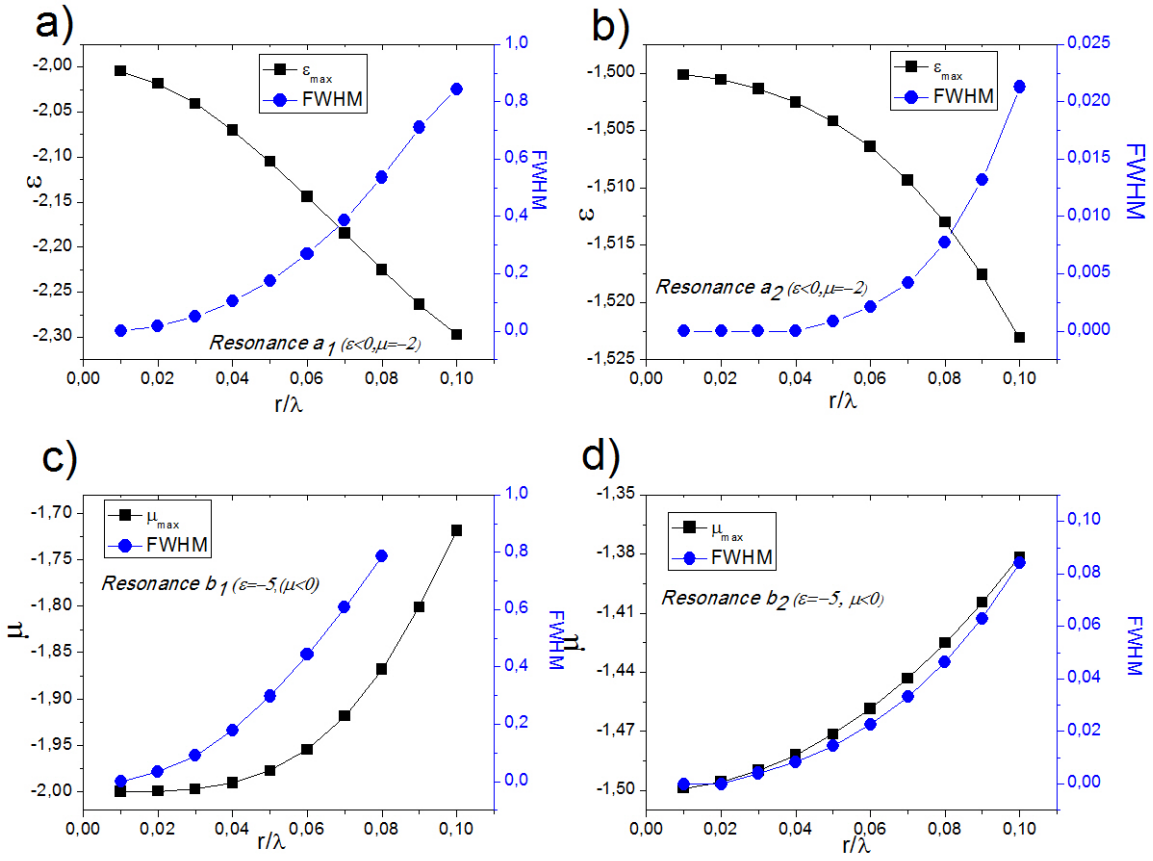

Figure 3.5: Evolution of the position and width (FWHM) of four representative resonances as a function of particle size

well-defined peak for the highest value of R. Similar behavior can be observed along the pure magnetic resonances (b_1 and b_2) in Figure 3.4(b). As R increases, the modes' position shifts while the shape becomes less sharp and broader. For the highest value of R, the dipolar one has almost disappeared and only the quadrupolar resonance is still present. Here, in opposition to the behavior explained in Figure 3.4(a), the quadrupolar mode is still observed for the lowest value of the particles size and also, as R increases,Q_{ext} takes higher values in the background, while in the peak it is lower.

This brief analysis can be made in more detail, even using the simple expressions for the Lorenz-Mie coefficients introduced by us (equations (2.66), (2.67) and those corresponding to b_1 and b_2), for a wide range for particle sizes. In Figure 3.5, the position (defined as the value of ϵ, for the electric modes, or μ, for the magnetic ones, for which the extinction efficiency is maximum) and the width (defined as the full width at half maximum, FWHM) of

the previous resonances are presented as a function of particle size. As before, the analyzed resonances are those appearing in the negative-negative range when the Lorenz-Mie coefficients, a_1, a_2, b_1 and b_2, take maximum values. The position of the resonances was analyzed for a permeability $\mu = -2$ and as a function of the permittivity, ϵ (Figures 3.5 (a) and (b)) while that of the magnetic modes was studied as a function of the permeability, μ, and a fixed permittivity $\epsilon = -5$ (Figures 3.5 (c) and (d)). The position of the electric resonances evolves in a similar way, as *R* increases the position of the peaks shifts to higher values of $|\epsilon|$ (red shift). The shift of the dipolar resonance, Figure 3.5(a), is from $\epsilon = -2$ to $\epsilon = -2.3$ while that of the quadrupolar one, Figure 3.5(b), is shifted from $\epsilon = -1.5$ to $\epsilon = -1.525$. Then, the dipolar resonance with a 15% shift is much more sensitive to particle size than the quadrupolar mode with a 1.6% shift.

These results are quite similar to those presented by M. Meier and A. Wokaum [93]. The authors explained that the red-shift of the resonances is produced by the dynamic depolarization, whereas the decrease in magnitude and broadening are due to radiation damping effects.

The evolution of the position for the magnetic resonances as the particle size increases differs from that of the electric ones. In both cases, for the dipolar magnetic (Figure 3.5(c)) and the quadrupolar magnetic (Figure 3.5(d)) resonances, as *R* increases the peak tends to lower values of the modulus of the magnetic permeability ($|\mu|$). The magnetic resonances evolves in the opposite direction to the electric ones as the particle size changes. This fact can also be observed in Figure 3.4(a), where the peak associated to the dipolar magnetic term (b_1) shows a shift opposite to the ones presented by the electric peaks. As in the previous case, the dipolar resonance suffers a larger shift (from $\mu = -2.0$ to $\mu = -1.75$) than the quadrupolar one (from $\mu = -1.5$ to $\mu = -1.38$) as particle size changes from $R = 0.01\lambda$ to $R = 0.1\lambda$. However, the difference between the dipolar shift (12.5%) and the quadrupolar one (8%) is much smaller than for the electric modes.

Concerning the resonance width (*FWHM*) in Figures 3.4 and 3.5, it is clear that for every case we analyzed, the smaller the particle size, the narrower the resonance peak. In other words, the slope of the evolution of the width with the particle size is positive for the four studied cases in figure 3.5. It is also interesting to remark from Figures 3.4 and 3.5 that the dipolar resonances are broader than the quadrupolar ones. The electric quadrupolar mode, related to a_2, is the narrowest. It is even difficult to observe for particle sizes lower than 0.05λ because, from figure 3.5(d), the FWHM of this resonance is almost zero for these values of *R*.

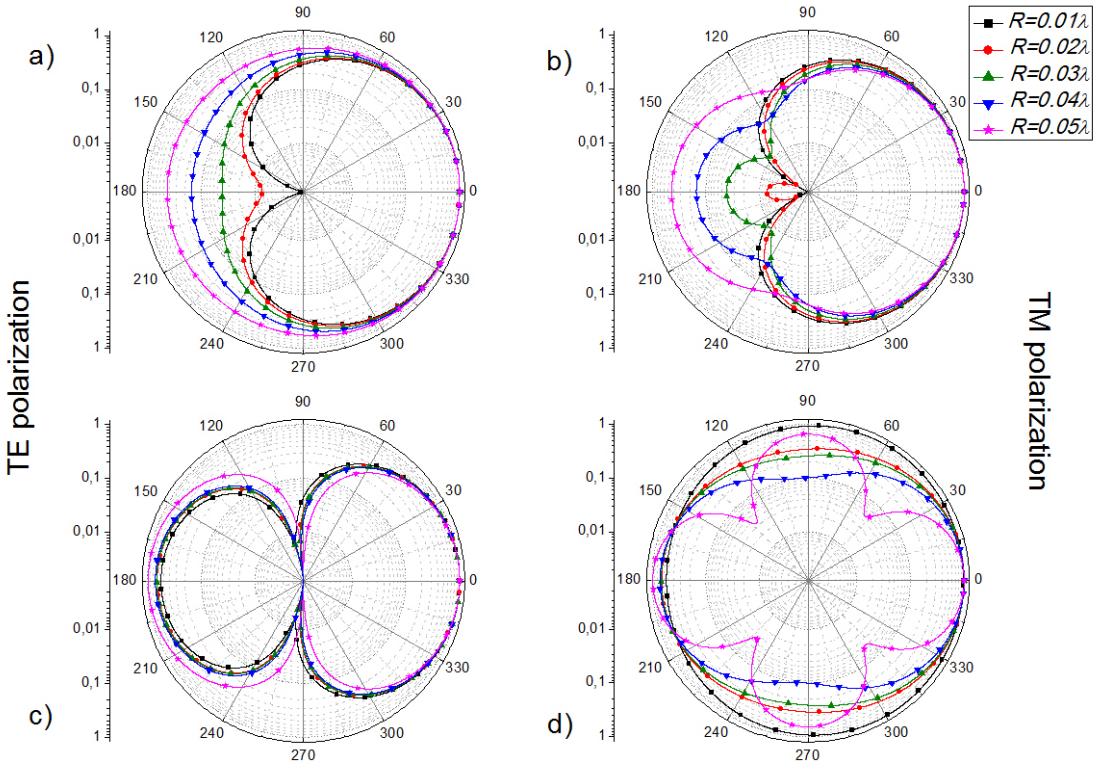

Figure 3.6: Normalized scattering diagrams when the electric dipolar, (a) and (b), and the electric quadrupolar, (c) and (d), resonance is excited for different particle sizes. The left figures correspond to a TE incident polarization while the right figures to a TM incident polarization

3.5. Scattering Diagrams for Resonant Situations

Another interesting feature of a resonant scatterer is the spatial distribution of the light scattered by it. In this section we will focus on the analysis of the far-field scattering patterns for small spherical particles with different sizes and optical properties when they are under resonant conditions.

For this we have used the approximations of the first four Mie coefficients we introduced in the previous chapter. As it was noted previously, these expressions reproduce the exact results accurately for particle sizes lower than 0.1λ. In this section, scattering diagrams for particles with sizes smaller than 0.05λ will be considered, since for higher values of R resonances are not well defined (see figure 3.4) and no remarkable feature is observed.

In Figures 3.6 and 3.7, the scattering diagrams are represented when the electric and magnetic resonances are excited respectively, for five different values of the particle size

	TE		*TM*	
R $\setminus \lambda$	**Dipolar**	**Quadrupolar**	**Dipolar**	**Quadrupolar**
0.01	0.05418(0°)	0.01234(0°)	0.05418(0°)	0.01234(0°)
0.02	0.06131(0°)	0.0187(0°)	0.06131(0°)	0.0187(0°)
0.03	0.07554(0°)	0.02087(0°)	0.07554(0°)	0.02087(0°)
0.04	0.09727(0°)	0.02088(0°)	0.09727(0°)	0.02088(0°)
0.05	0.09961(0°)	0.20629(0°)	0.09961(0°)	0.20629(0°)

Table 3.1: Maximum value of the intensity of the scattered light by a small sphere as a function of its size and for both incident polarizations, when an electric resonance is excited. Between parenthesis, we include the angle for which the maximum occurs.

($R = 0.01\lambda, 0.02\lambda, 0.03\lambda, 0.04\lambda$ and 0.05λ). The incident beam was taken to be linearly polarized with the incident electric field parallel (TM incident polarization) or perpendicular (TE polarization) to the scattering plane. In both figures, the plots on the left were calculated for a TE incident polarization while the ones on the right for a TM incident polarization.

The optical properties are chosen such that the described resonances are excited. The values of the permittivity (figure 3.6 (a)) and of the permeability (figure 3.6 (b)) cover an interval in which -2 is included. Here, the dipolar electric resonance is excited (remember that the exact position of the resonance changes with the particle size). In Figures 3.6 (c) and (d), the scattering diagrams correspond to the quadrupolar electric resonance ($\epsilon \simeq -1.5$ and $\mu = -2$, following those values observed in figure 3.4). Just as we pointed out before, the exact value of ϵ for which the resonance is excited, is different for every particle size. It is important to remark that when $\mu = -2$, the dipolar magnetic resonance is excited, as can be seen in figure 3.2(b). In spite of this, the electric resonances dominate in these particular cases while the magnetic resonance increases the background.

Similar situations are considered for the magnetic resonances, for which the scattering patterns are plotted in figure 3.7. Plots 3.7(a) and 3.7(b) correspond to the dipolar magnetic resonance, associated with coefficient b_1 ($\epsilon = -5$ and $\mu \simeq -2$). Figures 3.7 (c) and (d), as well, are associated with the excitation of the quadrupolar magnetic mode, related to high values of b_2 ($\epsilon = -5$ and $\mu \simeq -1.5$ depending on the radius of the particle).

Since we are mainly interested in the shape of the diagrams, we do not include the exact values of the optical properties. Furthermore, in order to analyze properly the angular structure of the scattered intensity as a function of particle size and the optical properties,

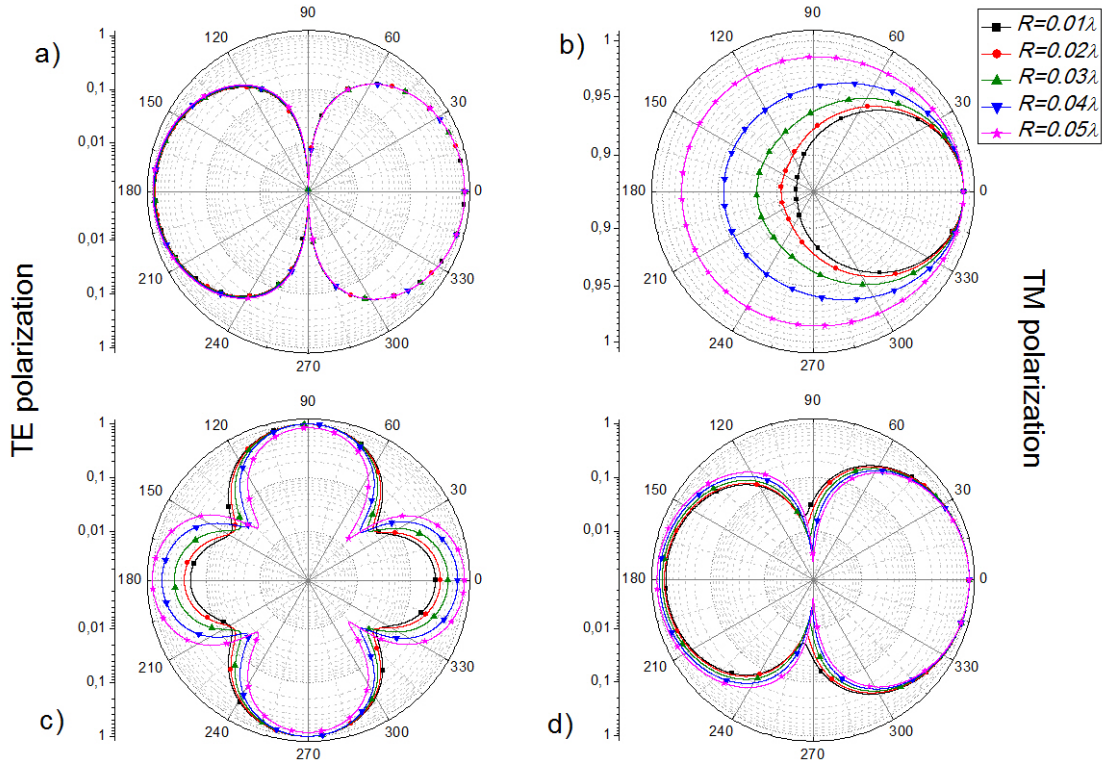

Figure 3.7: Normalized scattering diagrams when the magnetic dipolar, (a) and (b), and the magnetic quadrupolar, (c) and (d), resonance is excited for different particle sizes. The left figures correspond to a TE incident polarization while the right figures to a TM incident polarization

	TE		*TM*	
R $\setminus$ λ	**Dipolar**	**Quadrupolar**	**Dipolar**	**Quadrupolar**
0.01	0.05077(0°)	0.04527(90°)	0.05321(0°)	0.01299(0°)
0.02	0.05248(0°)	0.05163(90°)	0.05471(0°)	0.01799(0°)
0.03	0.05482(0°)	0.07001(270°)	0.05665(0°)	0.0436(0°)
0.04	0.05689(0°)	0.11177(270°)	0.05809(0°)	0.08278(0°)
0.05	0.05748(0°)	0.17536(180°)	0.05819(0°)	0.1762(180°)

Table 3.2: Maximum value of the scattered intensity by a small sphere as a function of its size and for both incident polarizations when a magnetic resonance is excited. Between parenthesis, we include the angle at which the maximum occurs.

all of the intensities are normalized to the maximum value (which is not necessarily in the forward direction). This makes an absolute comparison between sizes, optical properties or polarization very difficult. For further calculations or absolute comparisons, the values of the maxima are needed. This is why in tables 3.1 and 3.2, we have summarized the maximum values of the scattered intensity for every curve presented in Figures 3.6 and 3.7, respectively. The scattering angles at which the maximum appears are also included.

When the electric dipolar resonance is excited (see Figures 3.6 (a) and 3.6 (b)), the angular distribution of the scattered intensity evolves from "zero" backscattering for very small particle sizes to the typical shape for an electric dipole (isotropic for TE incident polarization and an eight-shape for TM polarization) for the highest size analyzed. The explanation of the "zero" backscattering for $R = 0.01\lambda$ is related to the fact that the electric dipolar resonance appears around $\epsilon \cong \mu \cong -2$. These values satisfy the zero backward condition, $\epsilon = \mu$, proposed by M.Kerker et al. [69]. As R increases, the resonance moves away from these values where Kerker's condition is satisfied and hence producing a higher signal in the backward direction and approaching to the dipolar scattering pattern. Moreover, when the $\epsilon = \mu$ condition is fulfilled, the scattering coefficients have the same amplitude and the angular distribution is equal for both polarizations. However, this TE-TM identity disappears as the scatterer becomes larger. As it was observed in Figure 3.4(a), the quadrupolar electric resonance is difficult to observe for very small particles because it is very narrow. Only for large particle sizes ($R \geq 0.3\lambda$) it can be observed. This fact is also observed in the scattering patterns. As it was remarked before, the quadrupolar electric resonance has been calculated for $\mu = -2$, at which the magnetic dipolar mode is also excited. For this reason and for TE incident polarization (Figure 3.6(c)), it is difficult to distinguish the dominating behavior because the angular distribution has the typical shape of an electric quadrupole and of a magnetic dipole. The TM polarization case (Figure 3.6(d)) is more interesting because the angular distribution evolves from the magnetic dipolar distribution (typical circular shape) for low size values to the electric quadrupolar cross-shape for the largest value of *R* analyzed. Again it can be seen that the quadrupolar character only dominates for large particle sizes while only the dipolar behavior can be observed for low particle sizes.

In Figure 3.7 we show polar diagrams of the scattered intensity when the magnetic resonances are excited: the dipolar in Figures 3.7(a) and 3.7(b) and the quadrupolar in Figures 3.7(c) and 3.7(d). It can be seen that the magnetic resonances do not give substantial information about the size dependence. When the magnetic dipolar mode is excited, the scattered intensity is distributed as for a typical magnetic dipole: an eight-shape for TE polarization and isotropically for a TM incident polarization, which is analogous to the electric dipole

but with the polarizations interchanged. The size-dependence evolution for TE polarization (Figure 3.7(a)) is hardly appreciated. However, for a TM polarization (Figure 3.7(b)) only a slight evolution from a predominantly forward scattering to a uniform scattering can be observed as R increases. From Figure 3.4(b), the quadrupolar magnetic resonance is well-defined even for very small particle sizes. As a consequence, the scattering diagrams present the typical profile of a magnetic quadrupole with the cross-shape for the TE incident polarization (Figure 3.7(c)) and an eight-shape for the TM polarization (Figure 3.7(d)). No noticeable changes of the scattering pattern can be observed as the particle's size increases, in this case.

3.6. Conclusions

In the last part of the previous chapter, we have proposed approximate expressions for the first four Mie coefficients, a_1, a_2, b_1 and b_2, for a spherical particle with electric and magnetic response and a radius lower than 0.1 times the incident wavelength.

The simplicity of these analytical expressions allows us to make a complete analysis of the Mie resonances all over the values of the optical properties: $\epsilon > 0$, $\epsilon < 0$, $\mu > 0$ and/or $\mu < 0$. The well-known resonances for very small spherical particles with $\epsilon > 0$ and $\mu = 1$ [139] have been reproduced accurately. We have also analyzed the evolution of these resonant modes as the magnetic permeability reaches values higher than 1, observing a shift towards lower values of the electric permittivity, in order to preserve the resonant condition.

Because of the recent interest in the field of the metamaterials and especially in the double-negative materials $(\epsilon < 0, \mu < 0)$ in the optical range, we have studied in detail the resonances that appear in this range. An interesting feature is the remarkable electric-magnetic symmetry that appears between the electric modes (dipolar, $\epsilon \sim -2$, and quadrupolar, $\epsilon \sim -1.5$) and the magnetic ones (dipolar, $\mu \sim -2$, and quadrupolar, $\mu \sim -2$).

Resonances depend strongly on the particle size. In this chapter, we have analyzed the dependence of two important characteristics of the modes: their position and width (*FWHM*) as a function of the radius of the particle. It could be seen that as R increases, resonances shift and become broader or less sharp, and for high values of R some resonances even miss their peak-shape. The evolution of the width as a function of particle size is general for all modes, but the shift direction and amplitude depends on the kind of resonance. For this reason, we have studied four different modes, that correspond high values of the Mie coefficients: a_1, a_2, b_1 and b_2.

Finally, we have studied the scattering diagrams for particles of different sizes and for resonant values of ϵ and μ. Particle sizes were chosen in the range $R \in [0.01, 0.1]\lambda$ this is $R \sim 10 - 100$ nm for visible wavelengths, i.e. nanometric particles. The evolution of the angular distribution of the scattered intensity is shown as a function of the particle size. As R increases, we have observed some interesting features: i) the zero backscattering ($\epsilon = \mu$) that appears at the electric dipolar resonance tends to disappear due to the shift of the resonance with the size increment, ii) the quadrupolar terms become more important than the dipolar ones and typical cross-shape diagrams appear and, iii) the scattering values are higher as particle increase its size, as was expected.

The study presented in this chapter is a numerical work carried out with values of the optical properties that don't correspond to any particular material available so far, but the simplicity and the generalization of the study of the resonances can be useful in the design of new materials in the optical range with important applications in fields like biomedicine, sensing or optical storage information.